



Black phosphorus nanosheets enhance differentiation of neural progenitor cells for improved treatment in spinal cord injury

Fumei He^a, Ke Cheng^a, Junyang Qi^a, Fangjie He^a, Chengjun Chu^b, Yue Xiong^a, Jingxin Zhao^a, JiaQi Ding^a, FanShu Kong^a, ZiMeng Cao^a, Gan Liu^{a,*}, Wenbin Deng^{a,*}

^a School of Pharmaceutical Sciences, Shenzhen Campus of Sun Yat-sen University, Shenzhen 518107, China

^b People's Hospital of Nujiang Lisu Autonomous Prefecture, Lushui City 673200, China



ARTICLE INFO

Keywords:

Black phosphorus nanosheets
Neural progenitor cells
Cell differentiation
Spinal cord injury
Axonal regeneration

ABSTRACT

Stem cell transplantation holds great potential as a treatment option for nerve damage diseases. However, the therapeutic effects are significantly impeded by low survival rate and uncontrolled differentiation of stem cells. In this study, black phosphorus nanosheets (BPNs), which are biodegradable inorganic nanomaterials, are first revealed with remarkable abilities to regulate cellular redox homeostasis, enhance transplant survival rate of stem cells, and facilitate neural differentiation of neural progenitor cells (NPCs). These effects of BPNs are proved to be associated with the activation of nuclear factor erythroid 2-like 2 (Nrf2) pathways in NPCs. *In vivo*, BPNs-treated NPCs could effectively inhibit inflammatory response and neuronal apoptosis in the mice with spinal cord injury (SCI). In addition, BPNs-treated NPCs more effectively reduce glial scar formation and promote axon regeneration compared with natural NPCs in SCI site. These findings collectively support the therapeutic potentials of BPNs for advanced stem cell transplantation and neural tissue engineering in the future.

1. Introduction

Nerve damage diseases, such as stroke and spinal cord injury (SCI), pose a serious threat to human health [1,2]. Due to the limited regenerative capacity of the central nervous system in the natural state, the fatality and disability rate of patients suffering from nerve injuries are extremely high [3]. In recent years, significant achievements have been made to promote nerve repair and functional recovery by using stem cells [4,5]. Stem cells demonstrate excellent self-renewal and differentiation ability and can repair damaged tissues through multiple pathways including cell replacement, secretion of soluble factors, and extracellular vesicles [6,7]. Despite these promising benefits, stem cell therapy still faces several limitations, with the most crucial problems being the poor survival rate and uncontrolled differentiation of stem cells *in vivo* [8]. To solve these problems, some strategies have been developed to improve the survival rate of transplanted cells and promote directional differentiation, including cytokines [9], small-molecule drugs [10], genetic modification [11], natural and synthetic nanomaterials [12–14], etc. Notably, nanomaterials serve as excellent carriers for functional groups, small-molecule drugs, and cytokines, which have been developed as a superior strategy for stem cell therapy [7,15].

Despite the advancements of these strategies, many problems, such as poor biological safety, complex preparation process, and technical cost, remain unsettled. To date, achieving a simple and feasible method to simultaneously improve the survival rate of stem cells and regulate their differentiation behavior has still been an ongoing challenge.

In recent years, black phosphorus nanosheets (BPNs), categorized as novel two-dimensional inorganic nanomaterials, have been widely used in the biomedical field [16,17]. Owing to excellent photothermal conversion efficiency and biodegradability, BPNs have been extensively applied in cancer therapies [18–21]. Interestingly, BPNs were also reported with remarkable effects on the treatment of neurological diseases [22–24]. Based on the inherent antioxidant capacity, electrical conductivity, and biodegradability of BPNs, three-dimensional black phosphorus nanoscaffolds were recently found with the ability to promote neural differentiation of stem cells and neural repair [22]. Despite these findings, the mechanism, therapeutics effects, and potential applications of BPNs on stem cell fate regulation, especially in neural stem cells (NSCs) are still unknown. Considering the great potential of nanomaterials for enhanced stem cell therapy and the potential therapeutic effects of BPNs on stem cells and neural repair, it is of great value and urgency to study the biological effects of BPNs on stem cells.

* Corresponding authors.

E-mail addresses: liugan5@mail.sysu.edu.cn (G. Liu), dengwb5@mail.sysu.edu.cn (W. Deng).

In our previous study, BPNs were revealed with excellent abilities to enhance the antioxidant capacity of stem cells by upregulating the nuclear factor E2-like 2 (Nrf2)-dependent antioxidant pathway, thus improving the survival rate of NPCs *in vivo* [25]. This provides great opportunities for the application of BPNs in stem cell therapy. Whereas, whether the pretreatment with BPNs affects the differentiation fate of stem cells is still unknown, considering that Nrf2 demonstrates an important impact on the stemness maintenance, self-renewal, and differentiation fate of stem cells [26,27]. Besides, Nrf2 activation was reported to promote osteogenic differentiation of mesenchymal stem cells [28–30]. Nrf2 overexpression could prevent the toxicity of amyloid β on NSCs and improve the survival, proliferation and differentiation of NSCs in mice [31]. In addition, transplantation of NSCs overexpressing Nrf2 also promoted stem cell regeneration of aging rats [32]. Based on these facts, it is probable that BPNs can regulate the differentiation of NPCs via the activation of the Nrf2 pathway.

Herein, we report that the direct treatment of BPNs can improve the survival rate of NPCs and enhance the neural differentiation of NPCs. These biological effects of BPNs on NPCs are comprehensively demonstrated and can be primarily attributed to the up-regulation of Nrf2 in NPCs induced by BPNs. To further explore the antioxidative effects on stem cells, passivated BPNs and phosphate solutions (mimicking BPNs degradation products) are utilized to reveal the effect of BPNs on neural differentiation of NPCs by regulating intracellular redox homeostasis. In SCI mice, BPNs are demonstrated with enhanced neuroprotection to NPCs. BPNs-treated NPCs effectively reduce glial scar formation and promote axon regeneration, demonstrating a better nerve repair effect. Our proposed biodegradable BPNs-based stem cell therapy provides more informative support for improving the efficacy of stem cell transplantation for nerve damage diseases (Fig. 1).

2. Materials and methods

2.1. Preparation and characterization of black phosphorus nanosheets

Black phosphorus crystal powder was purchased from Nanjing

MKNANO Tec Co., LTD. (Nanjing, China). The powder was dispersed in N-Methylpyrrolidone (NMP) solution, and then stripped off with an ultrasonic probe in ice water for 24 h. BPNs precipitates were obtained by centrifugation at 1000 rpm–4000 rpm and then dispersed in ultrapure water. Concentration of BPNs was determined at 460 nm using a UV-visible spectrophotometer (PerkinElmer). The morphology of BPNs was characterized by transmission electron microscopy (TEM, JEOL). The particle size distribution and zeta potential of BPNs were measured by dynamic light scattering (DLS, Brookhaven). Raman spectroscopy (Renishaw) was used to determine the characteristic absorption peak of BPNs. The characteristic peaks of azobenzoic acid-modified BPNs were measured by infrared spectroscopy.

2.2. Cell culture

NPCs were differentiated from human induced pluripotent stem cells (iPSCs), as previously reported [33], with the following components: 50% DMEM/F12 (GIBCO), 50% Neurobasal (GIBCO), 1x B27 (GIBCO), 1x N2 (STEMCELL Technologies), 1x GlutaMAX (GIBCO) and 10 ng/mL hLIF (Peprotech), 4 μ M CHIR99021 (MCE, HY-10182), 3 μ M SB431542 (MCE, HY-10431), 2 μ M Dorsomorphin (MCE, HY-13418A), and 0.1 μ M Compound E (MCE, HY-14176). At day 8, single cell passage was performed with ACCUTASE (Sigma-Aldrich), and the medium was switched to neural stem cell maintenance medium (NSMM: 1x B27, 1x N2, 1x GlutaMAX, 10 ng/mL hLIF, 3 μ M CHIR99021 and 2 μ M SB431542). In addition, it is necessary to add Y-27632 (MCE, HY-10071) at a final concentration of 10 μ M during each cell passage [25]. Neuronal differentiation was performed in DMEM/F12, 1x N2, 1x B27, 300 ng/mL cAMP (Sigma-Aldrich), 200 μ M vitamin C (Sigma-Aldrich), 10 ng/mL brain derived neurotrophic factor (BDNF) and 10 ng/mL glial cell derived neurotrophic factor (GDNF) (Peprotech).

2.3. Cell viability test

Cell viability was assessed by using the CCK-8 assay (APExBIO). In brief, Matrigel solutions containing gradient concentrations of BPNs

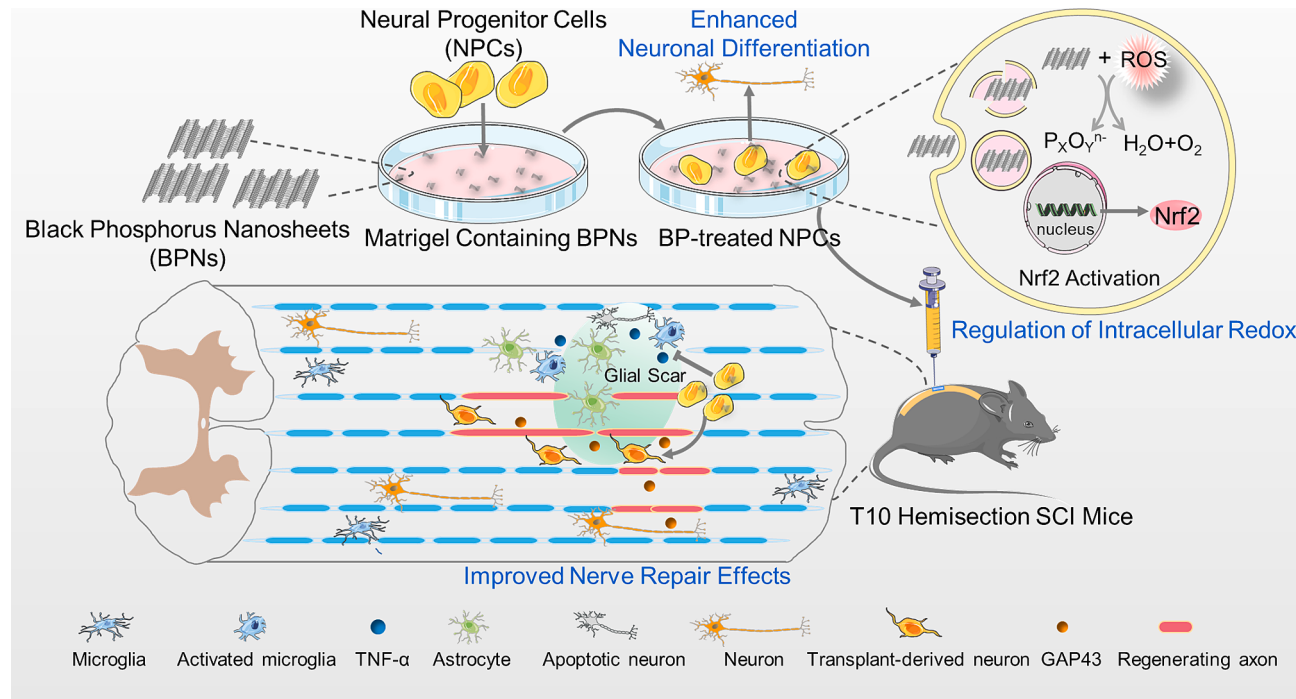


Fig. 1. Schematic illustration shows that BPNs enhance the neural differentiation of NPCs and improve axonal regeneration in SCI mice. BPNs promote neural differentiation of NPCs through the upregulation of Nrf2 expression and intracellular redox homeostasis. BPNs-treated NPCs have higher survival rate and neuro-protective effects *in vivo*.

were prepared and added to 96-well plates at a volume of 100 μL per well. The plates were incubated in a cell incubator for 1 h. NPCs were then seeded onto Matrigel-coated plates at a density of 10,000 cells per well and cultured for 5 days under normal conditions. Subsequently, the CCK8 test was performed: the culture medium was removed, and CCK8 working solution (10 μL of detection solution added to 100 μL of medium) was added. The cell plates were incubated in the dark for 2 h. The absorbance was measured at 450 nm to calculate the corresponding cell survival rate.

2.4. Intracellular distribution of BPNs

BPNs and excess of Coumarin 6 were put into a brown glass bottle, and NMP solution was added. The mixture was sealed and protected from light to stir for 48 h at room temperature (RT). At the end of the reaction, the free Coumarin 6 was removed by washing 3–5 times with NMP solution, and then washed 3 times by centrifugation with sterile water before dispersing in sterile water. NPCs were seeded in a confocal dish, and when the cell density reached about 56%–60%, the medium containing Coumarin 6-modified BPNs was added. After incubation in the dark for a period (3 h, 6 h, 12 h, 24 h), the medium was discarded. Lysotracker™ Red DND-99 (Thermofisher L7528) at a final concentration of 100 nM was added and incubated in the dark for 30 min. 4% paraformaldehyde solution was added and fixed at RT for 15 min. The cell nuclei were stained with DAPI for 10 min. An appropriate amount of anti-fluorescence quench agent was added, and the stained were stored in the dark at 4°C. The intracellular distribution of BPNs was observed by confocal microscopy.

2.5. Azobenzoic acid passivated BPNs

BPNs and excess p-Azidobenzoic Acid were put into the reaction flask, and an appropriate amount of N, N-dimethylformamide solution (DMF) was added. The reaction was carried out at 140°C for 12 h in the absence of oxygen and water. After the reaction, the precipitate was washed 3–5 times with DMF solution, once with ethanol, and then 3 times with sterile water. The precipitate was dispersed in sterile water and lyophilized for storage.

2.6. Measurement of intracellular phosphate ion concentration

When the density of NPCs reached about 70%, different concentrations of BPNs, BPNs-ABA, and different concentrations of phosphate solution were added. After 6 h, the cells were collected in 1.5 mL centrifuge tubes. The cells were washed 3 times with ultrapure water to adequately remove the phosphate from the medium, followed by resuspension of the cells with ultrapure water and the cells were placed in liquid nitrogen immediately. After 15 min, the cells were melted in a 37°C-water bath and immediately placed in a –80°C refrigerator. After 60 min, the cells were thawed in a 37°C water bath and freeze-thaw were repeated twice. Repeated freeze-thaw was performed to sufficiently lyse the cells to release intracellular phosphate ions. The supernatant was obtained by centrifugation at 12,000g for 10 min, and the phosphate ion concentration in the supernatant was detected by the phosphate detection kit (Beyotime, S0169S).

2.7. RNA isolation and qPCR

Total RNA was extracted from the cells using RNA extraction kit (EZBioscience, B0004D), and the concentration of RNA was determined using Nanodrop (Thermo Scientific), followed by cDNA obtained using a reverse transcription kit (TransGen Biotech, EasyScript® All-in-One First-Strand cDNA Synthesis SuperMix for qPCR (One-step gDNAR-removal)). The cDNA obtained was used for subsequent qPCR (TransGen Biotech, PerfectStart ® Green qPCR SuperMix). The real-time PCR machine (Roche, LightCycler) was preheated at 95°C for 5 min. There were

45 cycles of three-step amplification (denaturation at 95°C for 10 s, renaturation at 60°C for 10 s, and elongation at 72°C for 10 s). Melting (95°C denaturation for 10 s, 65°C denaturation for 60 s, 97°C denaturation for 1 s); the cells were cooled for 30 s at 37°C. The primers used for qPCR are shown in Table S1.

2.8. Western blotting (WB)

The protein was collected by centrifugation after the cells were fully lysed with RIPA lysate containing 1 mM PMSF (Beyotime). Protein concentration was determined using a BCA kit (Thermo Scientific). Equal amounts of proteins were separated by 10% sodium dodecyl sulfate-polyacrylamide gel electrophoresis (SDS-PAGE) (FUDE BioTech) at 200 V for 45 min after denaturation. The proteins on the gel were then transferred to a PVDF membrane in transfer buffer (0.3 mA for 90 min). After blocking with 5% fresh milk for 2 h, soaked in primary antibody at 4°C overnight. The next day, the samples were incubated with the corresponding HRP secondary antibody for 1 h. Band images were obtained by imaging system (baygene BG-gdsAUTO 730). Finally, Image J was used to calculate the gray value of the band. Primary antibodies: Rabbit anti-NOTCH1 antibody (1:1000, CST, D1E11), Rabbit anti-HES1 antibody (1:1000, CST, D6P2U), Mouse anti-GAPDH Monoclonal Antibody (1:1000, Proteintech, 60004-1-Ig). Second antibodies: Goat anti-Mouse IgG/HRP (1:2000, Bioss, bs-0296G-HRP), Goat anti-Rabbit IgG (H&L)-HRP (1:5000, Bioworld, BS13278).

2.9. Cell immunofluorescence

Adherent cells were fixed with paraformaldehyde for 15 min at RT, followed by membrane disruption with 0.2% TritonX100 for 15 min at RT. The cells were blocked with 1% BSA solution for 1 h at RT, and the appropriate primary antibody solution was added overnight at 4°C. The next day, the primary antibody was recycled, the corresponding secondary antibody was added, and the cells were incubated in the dark for 1 h. Nuclei were stained with DAPI (Solarbio). Finally, anti-fluorescence quencher (Solarbio) was added and photographed under fluorescence microscope (Nikon). Cellular fluorescence intensity and the proportion of positive cells were quantified using ImageJ software. Primary antibody includes: Mouse anti-NESTIN (1:500, Cell Signaling Technology (CST), 33475 s), Rabbit anti-PAX6 (1:200, CST, 60433 s), Rabbit anti-SOX2 (1:400, CST, 3579 s), Rabbit anti- β 3-Tubulin (1:200, CST, 5568 s), Rabbit anti-MAP2 (1:200, CST, 4542 s), Rabbit anti-GAP43 (1:200, CST, 8945 s), Rabbit anti-Synapsin-1 (1:200, CST, 5297 s), Rabbit anti-NEUN (1:50, CST, D4G4O), Rabbit anti-NF200 (1:200, Sigma-Aldrich, N4142), Mouse anti GFAP (1:400, Sigma-Aldrich, G6171), Mouse anti-STEM121 (1:500, TaKaRa, Y40410). Secondary antibody includes: Donkey anti-mouse IgG Secondary antibody, Alexa Fluor Plus 488 (1:500, Thermo Scientific, A32766) and Donkey anti-Rabbit IgG Secondary antibody, Alexa Fluor Plus 594 (1:500, Thermo scientific, A32754).

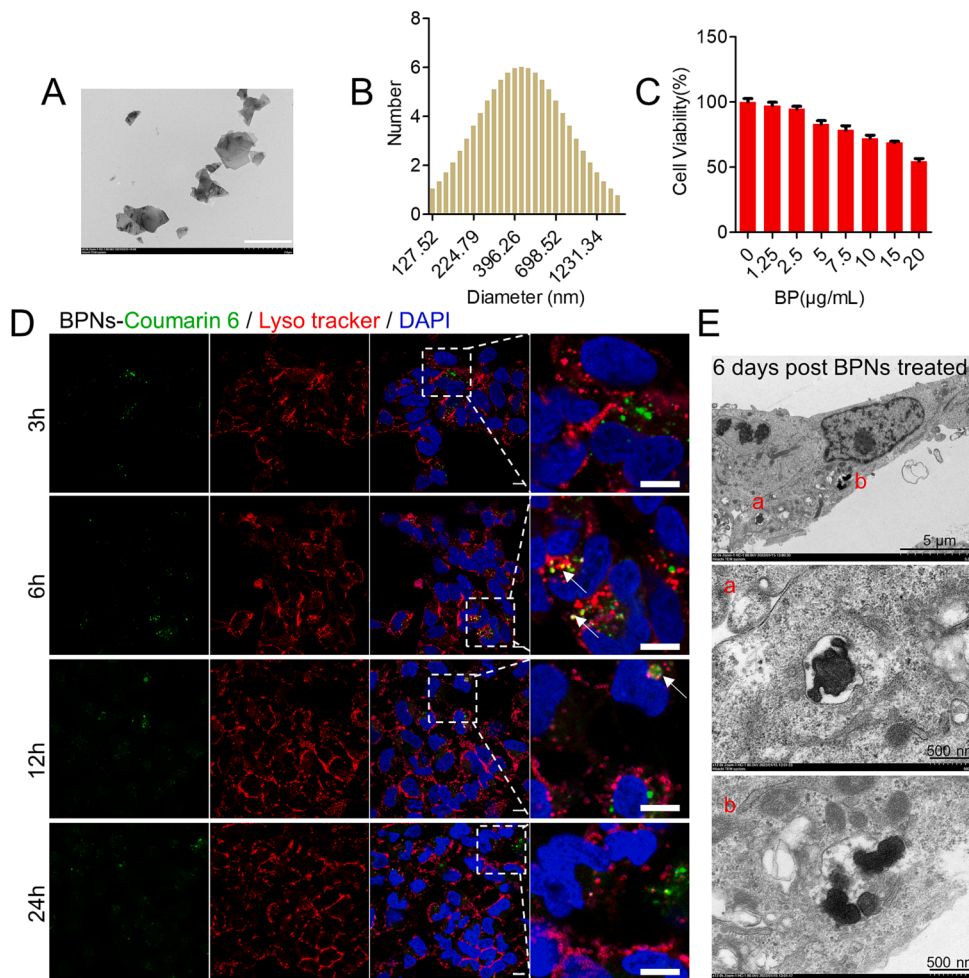
2.10. Spinal cord injury model and cell transplantation

All research protocols related to animal experiments were approved by the experimental Animal welfare ethical approval of the Experimental Animal Management and Use Committee of Wuhan Sevier Biotechnology Co., LTD. Briefly, Adult female C57BL/6 mice were anesthetized by intraperitoneal injection of pentobarbital (10 mg/kg), the surgical site was sterilized after shaving, and the mice were fixed in the prone position. Locating thoracic vertebrae 10 (T10) and a straight incision was made on the back corresponding to thoracic vertebrae 9–11, and the muscles were stripped to fully expose the vertebral plate. The T10 vertebral plate was removed, and the T10 spinal cord was exposed and lifted upward. The left half of the T10 segment of the spinal cord was cut from the midline of the spinal cord, and the left foot of the mouse immediately went limp. The cells were thawed and dispersed in

DMEM/F12 medium. Each mouse was injected with 5×10^5 cells (volume: 10 μL), and the model group was injected with the same volume of DMEM/F12 medium. Intramuscular injection of penicillin (1×10^4 units/mouse) was performed within one week after operation. Prevention of urinary tract infections requires urination twice a day. All mice were injected with cyclosporin A (10 mg/kg) from the day before surgery until the end of the experiment.

2.11. Immunofluorescence and immunohistochemical staining of paraffin sections

The paraffin sections of the spinal cord were deparaffinized and antigen retrieved before immunofluorescence staining and immunohistochemical staining. Immunohistochemistry requires blocking endogenous peroxidase with 3% H_2O_2 solution. This was followed by blocking with 3% BSA solution for 30 min at 37°C. After that, the appropriate primary antibody was added at 4°C overnight. The next day, the primary antibody was recycled, the corresponding secondary antibody was added, and the cells were incubated in the dark for 1 h. After that, the tissue autofluorescence was eliminated with a kit (Vectorlabs), and then the nuclei were stained with DAPI. Finally, anti-fluorescence quenching agent was added for sealing. Immunohistochemical staining was performed with HRP horseradish peroxidase labeled secondary antibody followed by DAB kit (Solarbio). The nuclei were stained with hematoxylin and the film were sealed with neutral gum after dehydration. The primary antibody used for immunohistochemistry: Rabbit anti-iba1 (1:250, WAKO, 019-19741). Secondary antibody: Goat Anti-Rabbit IgG (H + L) HRP (1:2000, Bioworld, BS13278).



2.12. Statistical analysis

All tests are repeated three times or more and the results are shown as mean \pm sem. All statistical analyses were performed using GraphPad Prism 5.0 software. For comparison of two groups, the two-tailed independent Student's *t*-test was used. For multiple groups, one-way analysis of variance (ANOVA) was used, **P* < 0.05, ***P* < 0.01, ****P* < 0.001.

3. Results and discussion

3.1. Characterization and intracellular distribution of BPNs

BPNs were prepared by the liquid phase stripping method [34] and gradient centrifugation in different size ranges. Our previous study demonstrated that BPNs with an average size of about 500 nm could significantly up-regulate Nrf2 expression in NPCs [25]. Hence, the average size of BPNs used in this study is around 500 nm, as shown in the Fig. 2A-B. BPNs demonstrated negligible toxicity to NPCs in low concentrations (Fig. 2C), suggesting the excellent biosafety of the BPNs concentration used in this study (normally 2.5 $\mu\text{g/mL}$, 80 μM). Before exploring the biological effects of BPNs on NPCs, the intracellular distribution of BPNs was characterized. To study the intracellular distribution of BPNs, a fluorescent dye, Coumarin 6, was loaded on BPNs by electrostatic adsorption. Cells were incubated with BPNs for 3 h, 6 h, 12 h, and 24 h, respectively. Next, lysosomes were labeled with lysosome tracker, and nuclei were stained with DAPI before cells were observed by a confocal microscope. As shown in Fig. 2D, for cells treated with BPNs

Fig. 2. Characterization and intracellular distribution of BPNs. A) TEM image of BPNs. Scale bar: 2 μm . B) Size and distribution of BPNs were measured by dynamic light scattering. C) The cell viability assay was performed with CCK8 after co-culture of NPCs with different concentrations of BPNs for 5 days ($n = 5$). D) The intracellular distribution of BPNs was recorded by confocal microscopy. Green represents coumarin-loaded BPNs, red represents lysosomes, and blue represents nuclei. Scale bar: 10 μm . E) TEM image of BPNs after 6 days of co-culture with NPCs.

for 3 h, a small amount of BPNs were absorbed by the cells and distributed in the cytoplasm, and almost no overlapping fluorescence signal was observed in lysosomes. After 6 h of incubation, the uptake of BPNs by the cells increased significantly, and the phagocytosis of BPNs

by lysosomes could be observed (as indicated in the white arrow). The longer uptake images indicated that the BPNs could escape from lysosomes and distribute in the cytoplasm [20]. TEM images of the cells treated with BPNs for 6 days showed that BPNs were remained in the

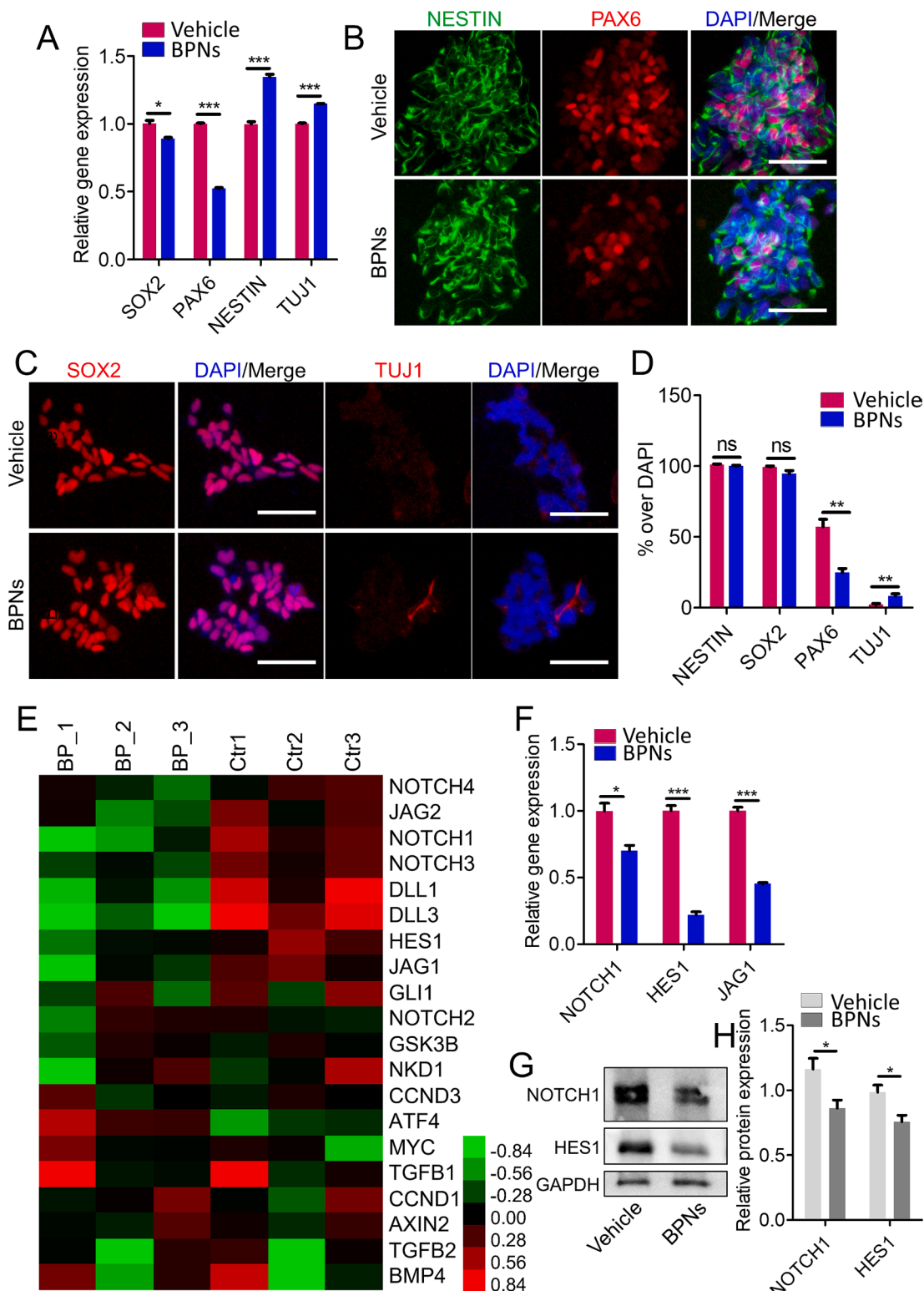


Fig. 3. BPNs promoted stemness loss and spontaneous differentiation of NPCs. A) qPCR validation of gene expression in NPCs treated with BPNs for 5 days ($n = 3$). B) Immunofluorescence staining and quantification of protein expression in NPCs treated with BPNs for 5 days. ($n = 4-5$). Scale bar: 100 μ m. E) RNA-seq heatmap showing the expression of genes of different signaling pathways in NPCs and BPNs-treated NPCs. F) qPCR validation of gene expression in NPCs treated with BPNs for 5 days ($n = 3$). G-H) WB validation of protein expression ($n = 3$). * $P < 0.05$, ** $P < 0.01$, *** $P < 0.001$.

cells (Fig. 2E). Moreover, the edges of the BPNs became smooth compared with the original form, likely due to the degradation process.

3.2. BPNs enhance neural differentiation of NPCs

3.2.1. BPNs promote the loss of stemness of NPCs

Our previous study demonstrated that BPNs could enhance the survival of stem cells under oxidative stress by up-regulating Nrf2 signaling pathway [25]. Nevertheless, it is still unclear whether the regulation of redox homeostasis of stem cells by BPNs affects the differentiation behavior of cells. To investigate the effect of BPNs on the differentiation of NPCs, first, we seeded NPCs on Matrigel containing BPNs and cultured NPCs in maintenance medium for 5 days. Then the marker genes of NPCs were detected by qPCR and immunofluorescence staining. As shown in the Fig. 3A-D, Surprisingly, BPNs significantly downregulated PAX6 expression. Considering PAX6 is a multifunctional transcription factor that regulates NSCs proliferation and differentiation [35], the down-regulation of PAX6 is an important signal for the loss of stemness in NPCs. Meanwhile, we detected the early neuronal marker (β -III Tubulin, TUJ1), and the percentage of TUJ1-positive cells in NPCs was increased by BPNs. In addition, RNA-seq data showed that BPNs downregulated the expression of genes involved in NOTCH1 signaling pathway in NPCs (Fig. 3E). We further validated this result by qPCR and WB experiment (Fig. 3F-H). Both NOTCH1 and HES1 play important roles in maintaining the undifferentiated state of neural stem cells [36], and the decrease of NOTCH1 and HES1 expression further indicated the loss of stemness of NPCs. These results indicated that BPNs could induce spontaneous neural differentiation of NPCs under maintenance culture medium.

3.2.2. BPNs enhance neural differentiation of NPCs

We have demonstrated that BPNs were able to promote loss of stemness and neural differentiation of NPCs in maintenance medium. On this basis, we further investigated whether BPNs-treated NPCs have more efficient neural differentiation in the induced differentiation medium. Medium containing BDNF, GDNF, vitamin C and cAMP was used to induce neural differentiation of NPCs (Fig. S1A) [10]. First, NPCs were cultured on Matrigel containing BPNs for 5 days and then harvested and reseeded without the addition of BPNs. After 2 days of maintenance culture, NPCs were changed to induction medium to observe the effect of BPNs pretreatment on neural differentiation. qPCR results at days 4 and 7 of differentiation showed that the expression of growth-associated protein 43 (GAP43) was significantly higher in the BPNs-treated group (Fig. S1B). As an axonal membrane protein, an important function of GAP43 is to promote neuronal axonal growth and synaptic plasticity [37]. At 10 days of differentiation, BPNs-treated NPCs-derived neurons were more likely to aggregate into spheres and express higher levels of GAP43 (Fig. 4A, B). As indicated by the arrow, BPNs-treated NPCs formed neural synapses earlier. After counter-staining with MAP2 (neuronal marker protein) and GFAP (astrocyte marker protein), we found that the BPNs-treated cells expressed more MAP2, indicating that BPNs-treated NPCs could differentiate into neurons more quickly (Fig. 4C-D). At day 14, neurons derived from BPNs-treated NPCs formed more complex branching structures (Fig. 4E). Calcium imaging also demonstrated that neurons derived from BPNs-treated NPCs had higher intracellular calcium concentration, especially in the axon of neurons (Fig. 4F), suggesting a higher degree of differentiation in BPNs-treated NPCs, since there are almost no calcium positive cells in undifferentiated iPSCs and NPCs. These findings collectively supported that pretreatment with BPNs indeed promoted the neural differentiation of NPCs.

3.3. BPNs promote neural differentiation of NPCs via the activation of Nrf2 pathway

RNA-seq results showed that BPNs selectively increased the

expression of antioxidant genes related to Nrf2 (Fig. 5A). The role of Nrf2 in regulating neural differentiation of NPCs with BPNs was further investigated using a specific inhibitor of Nrf2, ML385. As shown in Fig. 5B, the expression of NFE2L2, the gene encoding Nrf2 protein, was significantly inhibited by ML385 at a concentration of 2 μ M. BPNs were able to counteract the inhibitory effect of ML385 to some extent, but ultimately could not rescue the down-regulation of NFE2L2. Meanwhile, ML385 significantly inhibited the neural differentiation of NPCs. Similarly, the promoting effect of BPNs on neural differentiation of NPCs was blocked when NFE2L2 was inhibited. In addition, pretreatment with H_2O_2 increased the expression of NFE2L2 in NPCs and also promoted the neural differentiation of NPCs (Fig. 5C). However, unlike BPNs, H_2O_2 rapidly induced intracellular ROS production [25], but BPNs did not increase ROS production in NPCs either within 6 h or for up to 5 days (Fig. S2). This indicated that the increased expression of NFE2L2 in BPNs-treated NPCs was not due to a rapid oxidative stress response, but rather a slow regulatory process. Together, these results suggested that the activation of Nrf2 pathways in NPCs by BPNs was responsible for the neural differentiation of NPCs.

3.4. BPNs promote NPCs neural differentiation by regulating cellular redox homeostasis

BPNs were absorbed by NPCs and distributed in the cytoplasm (Fig. 2D-E). As biodegradable BPNs have high reducibility, its intracellular oxidation and degradation process may play an important role in the regulation of stem cell fate. To investigate the antioxidative mechanism of BPNs that leads to the promotion of neural differentiation of NPCs, a redox stable BPNs, BPNs-ABA, was prepared and tested. Based on previous methods [38], BPNs was covalently modification with azobenzoic acid (ABA) to offer the BPNs-ABA (Fig. S3A). The morphology and Zeta potential of BPNs-ABA were characterized by TEM and DLS respectively (Fig. S3B-D). BPNs-ABA shown an uneven surface compared to BPNs, and ABA further reduced the Zeta potential of BPNs. Next, the degradation rate of the two types of BPNs were then measured at 37°C. As shown in Fig. S3E-F, the degradation of BPNs-ABA was significantly slower than that of the BPNs. BPNs-ABA was more biocompatible than BPNs (Fig. S3G). This was consistent with the report that the rapid intracellular degradation of BPNs was one of the reasons for the cell cytotoxicity [18], which further proved that ABA passivation enhanced the stability of the BPNs.

Next, we compared the effects of BPNs and BPNs-ABA on the stemness of NPCs after 5 days under maintenance culture. As shown in the Fig. S3H, the two types of BPNs enhanced the expression of Nrf2, NES-TIN and TUJ1 of NPCs, but the expressions in BPNs-ABA group was significantly lower than that of BPNs group. Furthermore, the expressions of TUJ1 and MAP2 in BPNs group were higher than those in BPNs-ABA group after 5 days of neural differentiation induction (Fig. S3I). Immunofluorescence staining results at 10 days after neural differentiation showed that neurons derived from BPNs-treated NPCs had the most and longest neurofilaments (Fig. 5D-E). In addition, GAP43 expression was higher in BPNs-treated NPC group (Fig. 5D, F). To sum up, the enhanced stability and reduced redox capacity of BPNs after passivation led to the reduced promotion of neural differentiation of NPCs by BPNs. These results suggested that BPNs played an important role in the regulation of neural differentiation of NPCs by regulating the intracellular redox of stem cells.

Theoretically, the degradation of BPNs after cellular uptake will increase the local phosphate ion concentration (C-Pi). The cellular effects of the degradation products of BPNs on NPCs differentiation were then investigated by treating different types of phosphate mimics (H_3PO_4 , H_3PO_3 , H_3PO_2 , Na_2HPO_4 , Na_2HPO_3 , NaH_2PO_2) [20]. The intracellular C-Pi was measured after NPCs were treated with different concentrations of BPNs and phosphate solution for 6 h (Fig. 5G). The results showed that low concentrations of BPNs and phosphate solution did not increase the intracellular C-Pi, but high concentrations of phosphate

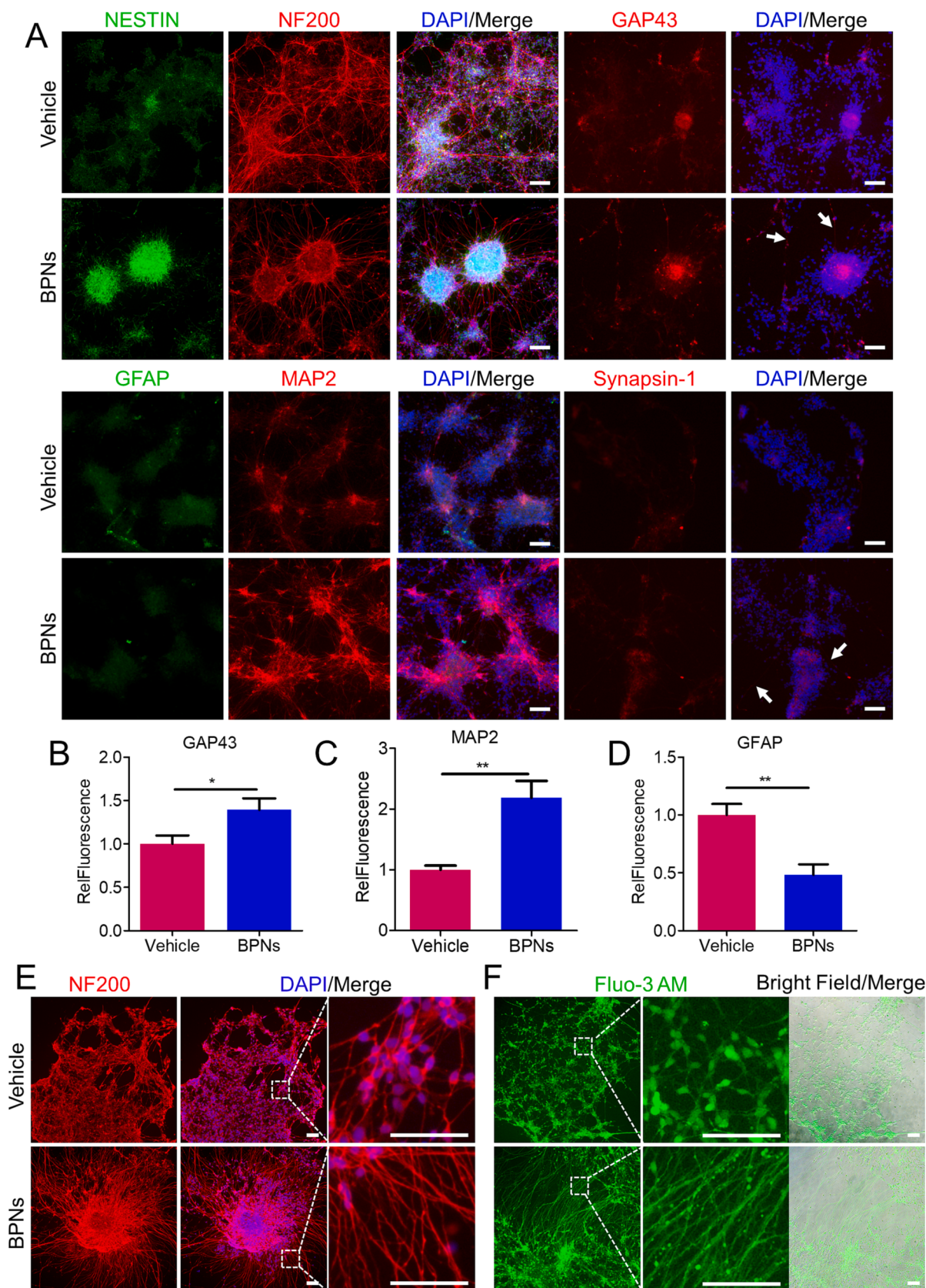


Fig. 4. BPNs enhanced neural differentiation of NPCs. A-D) Immunofluorescence staining and quantification of NPCs and BPNs-treated NPCs after 10 days of differentiation in neural differentiation medium ($n = 8$). Scale bar: 100 μ m. * $P < 0.05$, ** $P < 0.01$, *** $P < 0.001$. E) Immunofluorescence staining of NPCs and BPNs-treated NPCs after 14 days of differentiation in neural induction medium. Scale bar: 100 μ m. F) Calcium staining of NPCs and BPNs-treated NPCs after 14 days of differentiation in neural induction medium. Scale bar: 100 μ m.

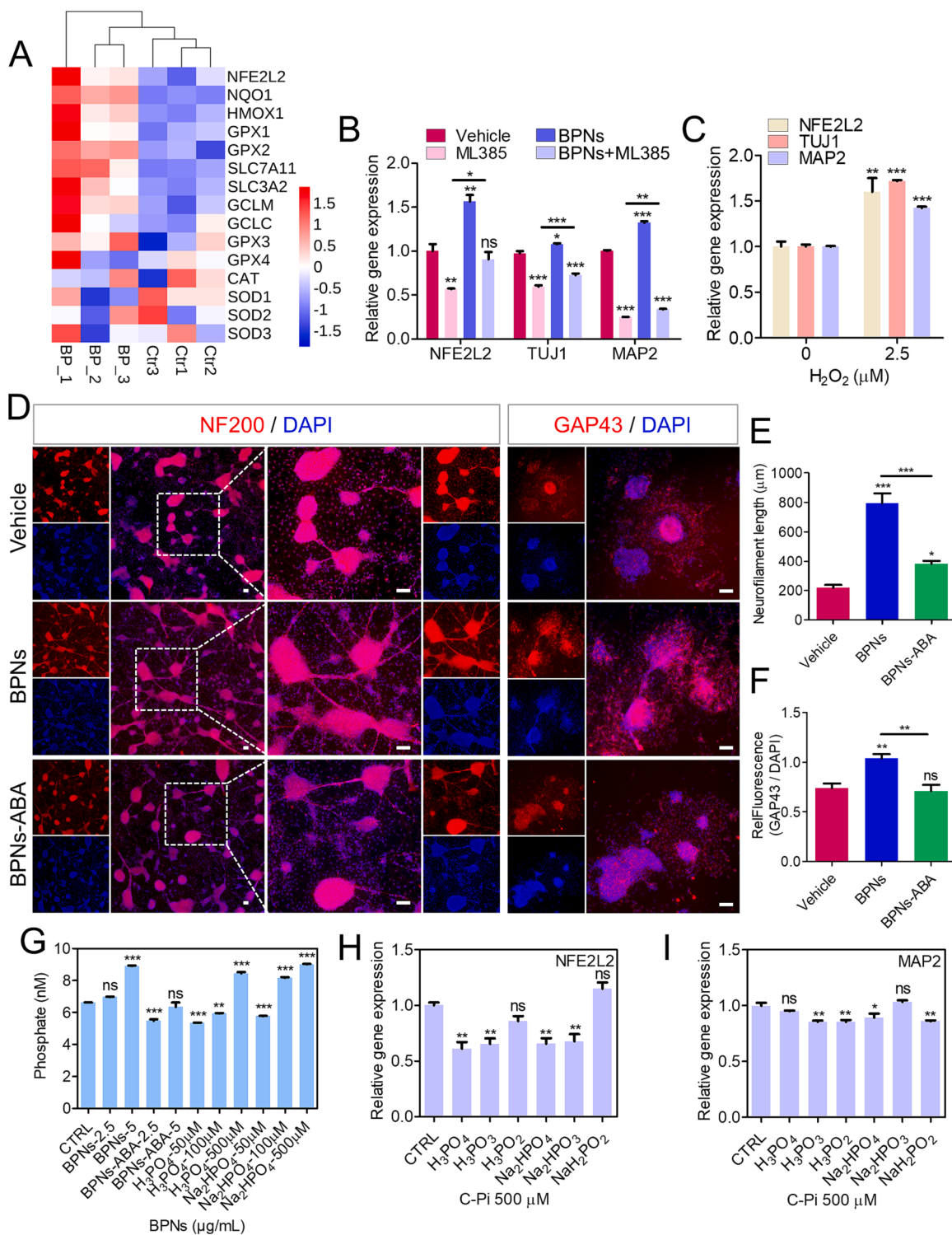


Fig. 5. BPNs promote neural differentiation of NPCs by regulating cellular redox homeostasis. A) Heatmap showing expression of antioxidation-related genes in NPCs and BPNs-treated NPCs. Heatmap analysis was performed online in BioLadder (bioladder.cn). B) Gene expression of NFE2L2, TUJ1 and MAP2 at 5 days of neural induction after ML385 and/or BPNs treatment of NPCs ($n = 3$). C) Gene expression of NFE2L2, TUJ1 and MAP2 at 5 days of neural induction after H_2O_2 treatment of NPCs ($n = 3$). D-F) Immunofluorescence staining and quantification of NPCs, BPNs- and BPNs-ABA-treated NPCs differentiated in neuronal differentiation medium for 10 days ($n = 4-5$). G) Different concentrations of BPNs, BPNs-ABA and phosphate solutions were incubated with NPCs for 6 h to detect the intracellular phosphate ion concentration ($n = 3$). H-I) Gene expression of NFE2L2 and MAP2 at 5 days after neural differentiation of NPCs treated with different species of phosphate at a final concentration of 500 μM ($n = 3$). * $P < 0.05$, ** $P < 0.01$, *** $P < 0.001$, ns. indicates nonsignificant difference.

increased the intracellular C-Pi significantly. Interestingly, the results of neural differentiation of NPCs treated with different phosphate for 5 days showed that neither 50 μ M nor 500 μ M phosphate could effectively increase the expression of NFE2L2 and MAP2 (Fig. S4 and Fig. 5H-I). These results indicated that exogenous phosphate did not promote neural differentiation of NPCs. The promotion of neural differentiation of NPCs is not depended on the degradation products of BPNs *in vitro*, but depended on the slow oxidative degradation process of BPNs in the cells.

3.5. BPNs enhance the neural repair effect of NPCs in SCI mice

In vitro experiments demonstrated that BPNs promoted the neural differentiation of NPCs by activating Nrf2 pathway and regulating the intracellular redox homeostasis. In addition, BPNs-treated NPCs expressed more GAP43 protein when differentiating into neurons. Considering that GAP43 protein is essential for axon growth and nerve regeneration, it is necessary to further apply BPNs to injured spinal cord models *in vivo* to promote axon regeneration effectively. We first established a mouse hemisection injury at T10 spinal cord segment (Fig. 6A-B), which resulted in immediate left hind limb paralysis.

In order to investigate the repair effect of NPCs on the acute phase of SCI, we transplanted cells shortly after the completion of modeling (the model group was injected with the same volume of DMEM/F12). As shown in the Fig. 6A, the entire experimental period was 42 days. BBB Neurologic scores [39,40] were performed at days 1, 3, 7, 14, 28, and 42 after cell transplantation (Fig. 6A, C). NPCs transplantation significantly improved the neurological score of mice with SCI, while the motor recovery of mice transplanted with BPNs-treated NPCs was significantly better than that of the natural NPC group and the model group, especially in the early stage (Fig. 6C), indicating that the pretreatment with BPNs could efficiently improve the therapeutic effect of NPCs on mice with SCI.

3.5.1. BPNs improve the survival rate of NPCs *in vivo*

Previous study suggested that BPNs-treated NPCs had a higher graft survival rate than natural NPCs in stroke rats [25]. On day 14 after cell transplantation, we performed immunofluorescence staining of the mice spinal cord with the antibody STEM121 that specifically recognizes human cytoplasm (Fig. 6E). The results showed that more STEM121 positive cells could be detected in the BPNs-treated NPC group (Fig. 6F). Surprisingly, the transplanted cells in BPNs-treated NPC group had stronger migration ability, not only at the injured site, but also at the distal uninjured area. We noticed that BPNs-treated NPCs were spindle/branched shape (as indicated by the white arrow, Fig. 6E), while the cytoplasm of the NPC group showed round dot shape, which also indicated that BPNs-treated NPCs had better cell viability and thus better migration ability.

3.5.2. The neuroprotective effect of BPNs-treated NPCs at the SCI site

Tissue integrity and inflammatory infiltration can be preliminarily known by H&E staining of the spinal cord of mice. As shown in Fig. 6D and Fig. 7A, the mice in the model group had atrophy of the caudal spinal cord after injury, resulting in incomplete and scattered sections. However, the two groups transplanted with NPCs retained complete spinal cord morphology. To gain further insight into neural damage at the SCI site, immunofluorescence staining of the spinal cord was performed for astrocytes (GFAP), neurons (NEUN) and synaptic protein (SYN-1) (Fig. 6D and Fig. S5). At the center of the lesion, the nerve tissue was so severely deficient that none of the three markers could be detected, while the lesion area was closely surrounded by astrocytes. The loss of a large number of neurons in the area of SCI site resulted in synaptic disruption. In the model group, almost no neurons were detected around the lesion area, while the NPCs transplanted groups had neurons around the lesion area. In particular, the BPNs-treated NPC group had the largest number of neurons around the lesion (Fig. 6H),

indicating that BPNs-treated NPCs provided more powerful neuroprotection for the SCI.

Inflammation plays an important role in the pathological response of SCI. Microglia are innate immune cells in the nervous system, which are considered to be the initiator and regulator of inflammation after injury, which can aggravate injury [41,42]. Ionized calcium-binding adaptor molecule-1 (Iba1: microglia marker) staining was used to detect microglia infiltration in the spinal cord at 14 days after transplantation. The morphology of highly activated microglia was swollen and heterogeneous [43]. As shown in Fig. S6A, although the tail end of the model group was tapered and atrophied leading to the loss of tissue samples, we could detect activated Iba1 positive cells from the injury site to the tail end (the part framed by the white line). The morphology of the spinal cord in the NPCs transplantation groups was relatively complete, and many activated microglia gathered in and around the injury site. The activation range of microglia in the model group was higher than that in the NPCs transplantation groups (Fig. S6B). Activated microglia can release a large number of inflammatory factors [24], so we further detected TNF- α expression. As shown in the Fig. 6G, I, in the injured area, the expression of TNF- α was significantly higher in the model group than in the NPCs transplantation groups. These results indicated that NPCs could effectively alleviate inflammatory infiltration in mice with SCI.

3.5.3. BPNs promote neural differentiation of NPCs *in vivo*

At 28 days after cell transplantation, we counterstained both the neuronal protein TUJ1 and the STEM121 antibody that specifically binds to human cytoplasm. As shown in the Fig. 7D, NPCs were mainly localized in the injured area, in which the BP-NPC group not only had more surviving cells, but also most of the cells expressed TUJ1 (Fig. 7E), indicating that the cells differentiated toward neurons. We also counterstained NPCs with Nrf2 and NESTIN antibody that specifically binds to human NSCs (Fig. 7F). The majority of surviving NPCs expressed Nrf2, and the positive rate of Nrf2 was higher in BPNs-treated NPC group (Fig. 7G). This was consistent with the results of neural differentiation of NPCs *in vitro*, indicating that the up-regulation of Nrf2 expression by BPNs significantly promoted the survival rate of transplanted NPCs and neural differentiation. In addition, Nrf2 was almost exclusively expressed in transplanted NPCs, and Nrf2-positive cells were not observed in the distal regions of the spinal cord. More importantly, the results of GAP43 Immunofluorescence staining in the positive area of the transplanted cells showed that BPNs-treated NPC group expressed more GAP43 (Fig. 7H), which further indicated that BPNs-treated NPCs had a higher degree of neural differentiation. The cells were still alive at 42 days after transplantation. In mice with severe spinal cord injury (neurological score: 2–3), NPCs were mainly localized at the lesion site. Most of the cells still expressed TUJ1 and Nrf2, and the BPNs-treated NPC group still had a higher positive rate. However, in the well-recovered mice (neurological score: 6–7), the surviving cells distributed in different regions of the spinal cord, and the positive rate of TUJ1, Nrf2, and NESTIN was significantly reduced (Fig. S7), indicating further differentiation of NPCs.

3.5.4. BPNs-treated NPCs reduce glial scar formation and promote axon regeneration

According to the neurological score of the mice, the motor function of the mice in different groups was significantly recovered at 28 days after cell transplantation (Fig. 6C). However, the mice showed extensive atrophy and thinning at the spinal cord injury site (Fig. 7A), especially in the model group, where the caudal atrophy resulted in incomplete and scattered spinal cord sections (Fig. 7B). As an axonal membrane protein, GAP43 is expressed at high levels during neuronal development and regeneration, and participates in neuronal synapse formation and nerve regeneration [37]. To assess the axonal regeneration in mice, GAP43 protein expression was detected. As shown in Fig. S8, the expression of GAP43 protein was significantly increased around the injured area in the

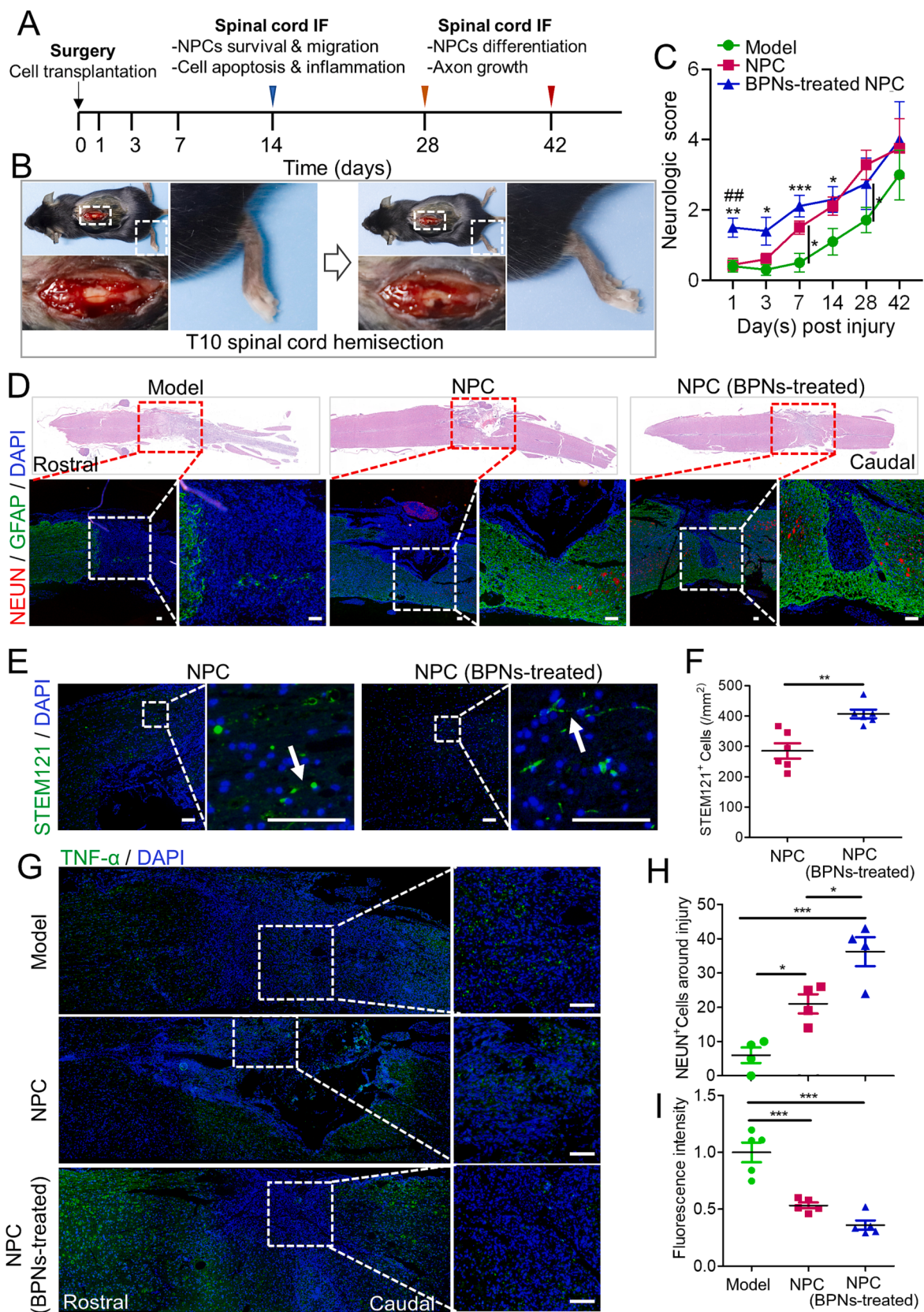


Fig. 6. BPNs-treated NPCs showed better neuroprotective effect on SCI in mice. A) Schematic diagram of the *in vivo* experiments. B) Schematic representation of the SCI model. C) Neurological scores of SCI mice at different time points ($n = 4-5$). 14 days after cell transplantation: D) H&E staining and Immunofluorescence staining of mice spinal cord. GFAP-labeled astrocytes and NEUN-labeled survival neurons Scale bar: 100 μ m. E-F) Staining and quantification of mice spinal cord specific for human cytoplasm ($n = 6$). Scale bar: 100 μ m. G) Immunofluorescence staining of inflammatory factors in mice spinal cord. Scale bar: 100 μ m. H-I) Immunofluorescence intensity was quantified for panels D and G ($n = 4-5$). * $P < 0.05$, ** $P < 0.01$, *** $P < 0.001$, ns. indicates nonsignificant difference.

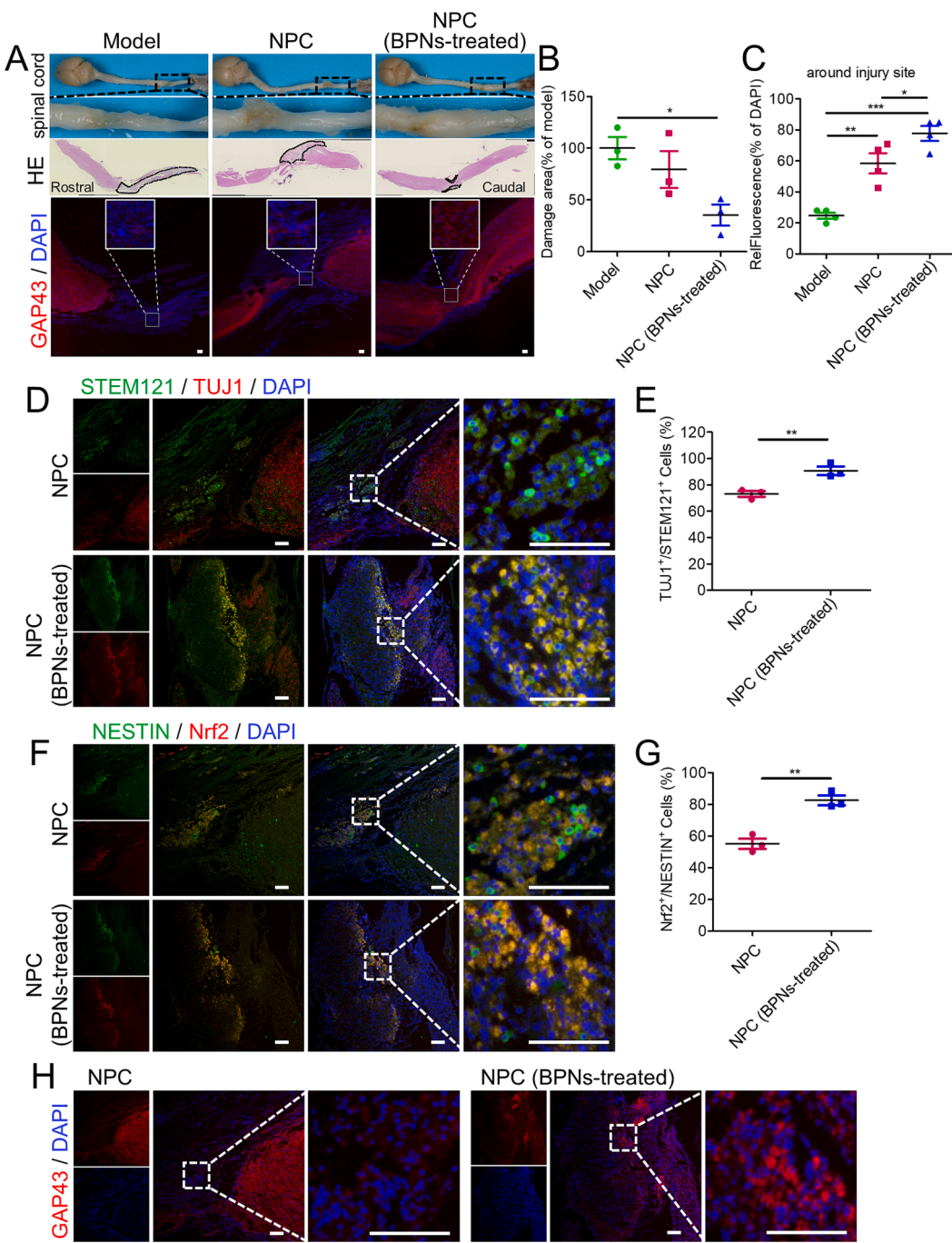


Fig. 7. BPNs promoted neural differentiation and GAP43 protein expression of NPCs *in vivo*. 28 days after cell transplantation, A) Morphology and H&E staining of spinal cord as well as GAP43 Immunofluorescence staining. Scale bar: 100 μ m. B) Quantification of tissue defect area in H&E staining in panel A ($n = 3$). C) Quantification of GAP43 immunofluorescence intensity in A ($n = 4$). D-G) The transplanted cells were marked with STEM121 and NESTIN, and the positive ratio of TUJ1 and Nrf2 in transplanted cells was observed, respectively ($n = 3$). Scale bar: 100 μ m. H) The expression of GAP43 protein was observed in the site where the transplanted cells survived. Scale bar: 100 μ m. * $P < 0.05$, ** $P < 0.01$, *** $P < 0.001$.

NPCs transplantation groups, indicating that the regeneration ability of axons was activated, while this phenomenon could not be seen in the model group. The quantitative results of GAP43 fluorescence intensity in the injured area showed that the BPNs-treated NPC group had the highest expression of GAP43 protein (Fig. 7C). More importantly, the transplanted cells in the BPNs-treated NPC group also expressed more GAP43 protein than the NPC group (Fig. 7H), which favored axon regeneration.

Axonal regeneration in the spinal cord was measured by co-staining GFAP and SYN1 at 42 days after cell transplantation (Fig. 8A). At this

stage, most spinal cord in the model group were still devoid of neural tissue and even failed to produce glial scars, while in the NPCs transplantation groups, the synaptic disconnection “gap” was filled by astrocytes (Fig. 8B). BPNs-treated NPC group had the shortest synaptic “gap” (Fig. 8C), and GAP43 staining demonstrated that this “gap” already expressed GAP43, implying that synaptic “bridges” were about to be established (Fig. 8A, D). These results collectively support that BPNs-treated NPCs indeed have a higher survival rate and neural differentiation *in vivo*, effectively inhibiting the inflammatory response and neuronal apoptosis at the site of SCI. In addition, it can promote axonal

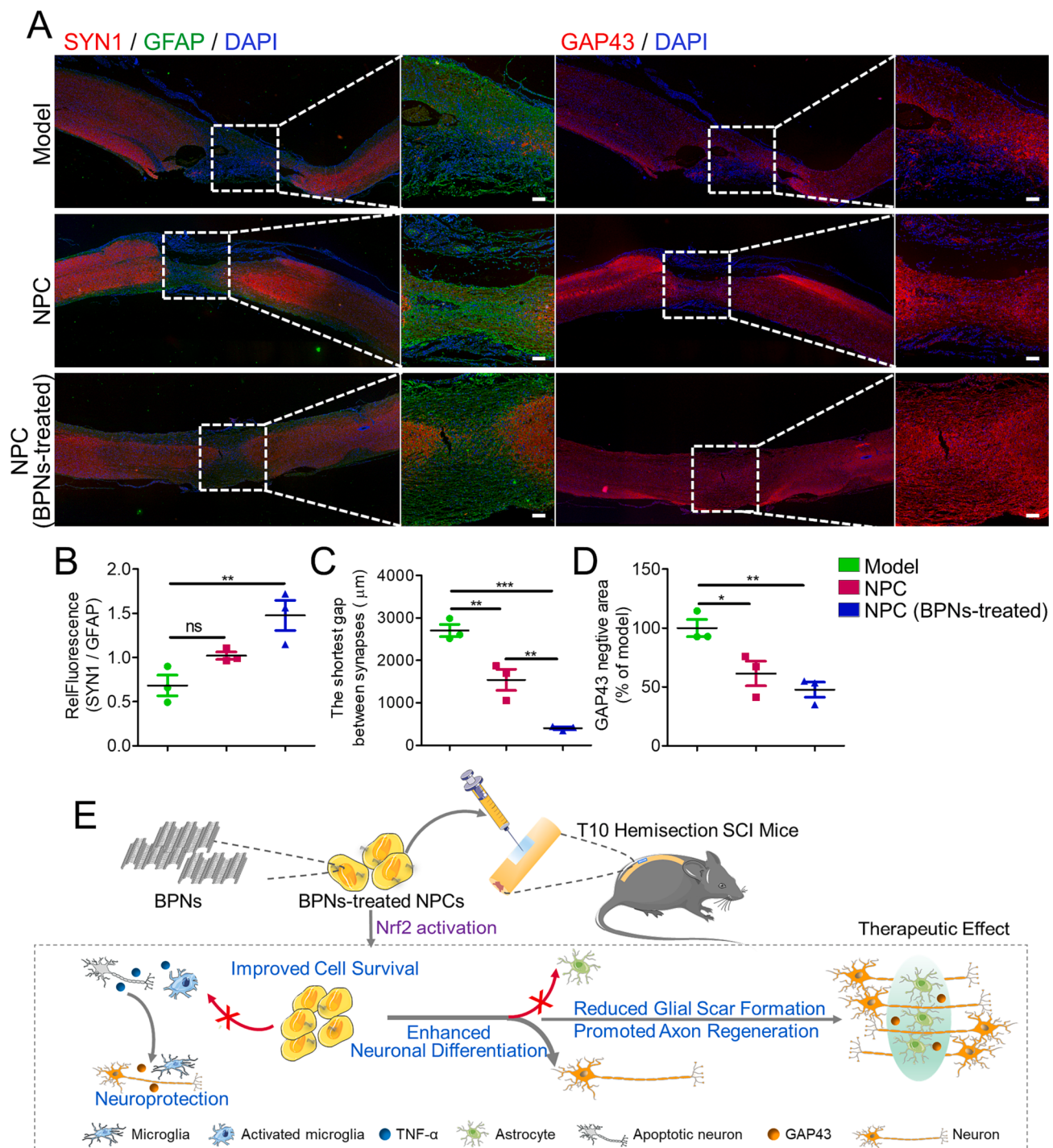


Fig. 8. BPNs-treated NPCs enhance axon regeneration in mice with SCI. A) Immunofluorescence staining targeting neural synapses (SYN1), astrocytes (GFAP), and axonal membrane proteins (GAP43) in mice spinal cord at 42 days after cell transplantation. Scale bar: 100 μm . In and around the lesion center: B) SYN1 to GFAP fluorescence intensity ratio. C) Relative area of low GAP43 expression. D) The shortest distance that can connect interrupted synapses in the spinal cord ($n = 3$). * $P < 0.05$, ** $P < 0.01$, *** $P < 0.001$, ns. indicates nonsignificant difference. E) Schematic diagram of BPNs enhancing the therapeutic effect of NPCs on SCI.

repair by bridging the injury (Fig. 8E).

4. Conclusions

In summary, this study uncovered the unique biological effects of BPNs on stem cells, including improving the graft survival of NPCs and promoting the neural differentiation of NPCs. The stem cell uptake and distribution of BPNs in NPCs were first monitored. BPNs were then applied to NPCs and the results demonstrated that BPNs were able to

promote the neural differentiation of NPCs in both maintenance and induced differentiation media. The mechanism of these effects was investigated and could be mainly attributed to the activation of Nrf2 signaling pathway by BPNs. Meanwhile, we verified the regulation of cellular redox homeostasis by BPNs was another potential mechanism for promoting the differentiation of NPCs. BPNs were applied to the mice model with spinal cord injury, and the results suggested that BPNs could improve the survival rate of NPCs and exhibit enhanced neuroprotection on NPCs and strong axon regeneration ability. BPNs as blank

nanocarriers could achieve excellent therapeutic effects in stem cell therapy. It's expected that the assembling of BPNs with gene vectors, growth factors, and small molecule drugs in the future could be a powerful tool to improve stem cell survival and induce their neuronal differentiation, thereby providing new insights into the treatment of neurological diseases.

Declaration of Competing Interest

The authors declare that they have no known competing financial interests or personal relationships that could have appeared to influence the work reported in this paper.

Data availability

Data will be made available on request.

Acknowledgements

We acknowledge financial support from Shenzhen Science and Technology Program (Grant No. KQTD20190929173853397), Science, Technology & Innovation Commission of Shenzhen Municipality (Grant No. JCYJ20180307154606793), National Natural Science Foundation of China (Grant Nos. 81772449 and 81971081), the Innovation and Technology Fund of Shenzhen (Grant No. JCYJ20180307154653332), the Innovation and Technology Fund of Guangzhou (201803010090).

Appendix A. Supplementary data

Supplementary data to this article can be found online at <https://doi.org/10.1016/j.cej.2023.144977>.

References

- [1] M.Y. Hathidara, V. Saini, A.M. Malik, Stroke in the young: a global update, *Curr. Neurol. Neurosci. Rep.* 19 (11) (2019) 91, <https://doi.org/10.1007/s11910-019-1004-1>.
- [2] S.B. Jazayeri, S.F. Maroufi, E. Mohammadi, M.A. Dabbagh Ohadi, E.M. Hagen, M. Chalangari, S.B. Jazayeri, M. Safrarian, S.A. Zadegan, Z. Ghodsi, V. Rahimi-Movaghar, Incidence of traumatic spinal cord injury worldwide: A systematic review, data integration, and update, *World Neurosurg.* X 18 (2023), 100171, <https://doi.org/10.1016/j.wnsx.2023.100171>.
- [3] P.M. George, G.K. Steinberg, Novel stroke therapeutics: unraveling stroke pathophysiology and its impact on clinical treatments, *Neuron* 87 (2) (2015) 297–309, <https://doi.org/10.1016/j.neuron.2015.05.041>.
- [4] R. De Gioia, F. Biella, G. Citterio, F. Rizzo, E. Abati, M. Nizzardo, N. Bresolin, G. P. Comi, S. Corti, Neural stem cell transplantation for neurodegenerative diseases, *Int. J. Mol. Sci.* 21 (9) (2020), <https://doi.org/10.3390/ijms21093103>.
- [5] T. Yasuhara, S. Kawauchi, K. Kin, J. Morimoto, M. Kameda, T. Sasaki, B. Bonsack, C. Kingsbury, N. Tajiri, C.V. Borlongan, I. Date, Cell therapy for central nervous system disorders: current obstacles to progress, *CNS Neurosci. Ther.* 26 (6) (2020) 595–602, <https://doi.org/10.1111/cns.13247>.
- [6] I. Fischer, J.N. Dulin, M.A. Lane, Transplanting neural progenitor cells to restore connectivity after spinal cord injury, *Nat. Rev. Neurosci.* 21 (7) (2020) 366–383, <https://doi.org/10.1038/s41583-020-0314-2>.
- [7] L.T. Yang, S.T.D. Chueng, Y. Li, M. Patel, C. Rathnam, G. Dey, L. Wang, L. Cai, K. B. Lee, A biodegradable hybrid inorganic nanoscaffold for advanced stem cell therapy, *Nat. Commun.* 9 (2018), <https://doi.org/10.1038/s41467-018-05599-2>.
- [8] S. Shah, P.T. Yin, T.M. Uehara, S.T.D. Chueng, L.T. Yang, K.B. Lee, Guiding stem cell differentiation into oligodendrocytes using graphene-nanofiber hybrid scaffolds, *Adv. Mater.* 26 (22) (2014) 3673–3680, <https://doi.org/10.1002/adma.201400523>.
- [9] B. Descamps, J. Saif, A.V. Benest, G. Biglino, D.O. Bates, A. Chamorro-Jorgues, C. Emanueli, BDNF (brain-derived neurotrophic factor) promotes embryonic stem cells differentiation to endothelial cells via a molecular pathway, including MICRORNA-214, EZH2 (enhancer of zeste homolog 2), and eNOS (endothelial nitric oxide synthase), *Arterioscler. Thromb. Vasc. Biol.* 38 (9) (2018) 2117–2125, <https://doi.org/10.1161/ATVBAHA.118.311400>.
- [10] W. Li, W. Sun, Y. Zhang, W. Wei, R. Ambasudhan, P. Xia, M. Talantova, T. Lin, J. Kim, X. Wang, W.R. Kim, S.A. Lipton, K. Zhang, S. Ding, Rapid induction and long-term self-renewal of primitive neural precursors from human embryonic stem cells by small molecule inhibitors, *PNAS* 108 (20) (2011) 8299–8304, <https://doi.org/10.1073/pnas.1014041108>.
- [11] S. Shah, A. Solanki, P.K. Sasmal, K.B. Lee, Single vehicular delivery of siRNA and small molecules to control stem cell differentiation, *J. Am. Chem. Soc.* 135 (42) (2013) 15682–15685, <https://doi.org/10.1021/ja4071738>.
- [12] S.T.D. Chueng, L.T. Yang, Y.X. Zhang, K.B. Lee, Multidimensional nanomaterials for the control of stem cell fate, *Nano Converg* 3 (2016), <https://doi.org/10.1186/s40580-016-0083-9>.
- [13] S.Y. Park, J. Park, S.H. Sim, M.G. Sung, K.S. Kim, B.H. Hong, S. Hong, Enhanced differentiation of human neural stem cells into neurons on graphene, H263+, *Adv. Mater.* 23 (36) (2011) <https://doi.org/10.1002/adma.201101503>.
- [14] A. Solanki, S. Shah, K.A. Memoli, S.Y. Park, S. Hong, K.B. Lee, Controlling differentiation of neural stem cells using extracellular matrix protein patterns, *Small* 6 (22) (2010) 2509–2513, <https://doi.org/10.1002/smll.201001341>.
- [15] T. Zhang, F. Li, Q. Xu, Q. Wang, X. Jiang, Z. Liang, H. Liao, X. Kong, J. Liu, H. Wu, D. Zhang, C. An, L. Dong, Y. Lu, H. Cao, D. Kim, J. Sun, T. Hyeon, J. Gao, D. Ling, Ferrimagnetic nanochains-based mesenchymal stem cell engineering for highly efficient post-stroke recovery, *Adv. Funct. Mater.* 29 (24) (2019) 1900603, <https://doi.org/10.1002/adfm.201900603>.
- [16] M. Luo, T. Fan, Y. Zhou, H. Zhang, L. Mei, 2D black phosphorus-based biomedical applications, *Adv. Funct. Mater.* 29 (13) (2019) 1808306, <https://doi.org/10.1002/adfm.201808306>.
- [17] J. Ouyang, C. Feng, X.C. Zhang, N. Kong, W. Tao, Black phosphorus in biological applications: evolutionary journey from monoelemental materials to composite materials, *Accounts Mater Res* 2 (7) (2021) 489–500, <https://doi.org/10.1021/accountsmr.1c00039>.
- [18] W. Zhou, T. Pan, H. Cui, Z. Zhao, P.K. Chu, X.F. Yu, Black phosphorus: bioactive nanomaterials with inherent and selective chemotherapeutic effects, *Angew. Chem. Int. Ed. Engl.* 58 (3) (2019) 769–774, <https://doi.org/10.1002/anie.201810878>.
- [19] S. Geng, T. Pan, W. Zhou, H. Cui, L. Wu, Z. Li, P.K. Chu, X.F. Yu, Bioactive phototherapy with black phosphorus for in vivo tumor suppression, *Theranostics* 10 (11) (2020) 4720–4736, <https://doi.org/10.7150/thno.43092>.
- [20] X.M. Shao, Z.H. Ding, W.H. Zhou, Y.Y. Li, Z.B. Li, H.D. Cui, X. Lin, G.L. Cao, B. H. Cheng, H.Y. Sun, M.Q. Li, K. Liu, D.Y. Lu, S.Y. Geng, W.L. Shi, G.F. Zhang, Q. L. Song, L. Chen, G.C. Wang, W. Su, L.T. Cai, L.J. Fang, D.T. Leong, Y. Li, X.F. Yu, H.C. Li, Intrinsic bioactivity of black phosphorus nanomaterials on mitotic centrosome destabilization through suppression of PLK1 kinase, 1150+, *Nat. Nanotechnol.* 16 (10) (2021) <https://doi.org/10.1038/s41565-021-00952-x>.
- [21] J. Qi, Y. Xiong, K. Cheng, Q. Huang, J. Cao, F. He, L. Mei, G. Liu, W. Deng, Heterobifunctional PEG-grafted black phosphorus quantum dots: “Three-in-One” nano-platforms for mitochondria-targeted photothermal cancer therapy, *Asian J. Pharm. Sci.* 16 (2) (2021) 222–235, <https://doi.org/10.1016/j.ajps.2020.09.001>.
- [22] Y. Qian, W.E. Yuan, Y. Cheng, Y.Q. Yang, X.H. Qu, C.Y. Fan, Concentrically integrative bioassembly of a three-dimensional black phosphorus nanoscaffold for restoring neurogenesis, angiogenesis, and immune homeostasis, *Nano Lett* 19 (12) (2019) 8990–9001, <https://doi.org/10.1021/acs.nanolett.9b03980>.
- [23] S. Xiong, Z. Li, Y. Liu, Q. Wang, J. Luo, X. Chen, Z. Xie, Y. Zhang, H. Zhang, T. Chen, Brain-targeted delivery shuttled by black phosphorus nanostructure to treat Parkinson's disease, *Biomaterials* 260 (2020), 120339, <https://doi.org/10.1016/j.biomaterials.2020.120339>.
- [24] W. Chen, J. Ouyang, X. Yi, Y. Xu, C. Niu, W. Zhang, L. Wang, J. Sheng, L. Deng, Y.-N. Liu, S. Guo, Black phosphorus nanosheets as a neuroprotective nanomedicine for neurodegenerative disorder therapy, *Adv. Mater.* 30 (3) (2018), 1703458, <https://doi.org/10.1002/adma.201703458>.
- [25] F. He, Z. Liu, J. Xu, Y. Xiong, X. Zhang, J. Qi, X. Lin, C. Chu, L. Shen, G. Liu, W. Deng, Black phosphorus nanosheets suppress oxidative damage of stem cells for improved neurological recovery, *Chem. Eng. J.* 451 (2023), 138737, <https://doi.org/10.1016/j.cej.2022.138737>.
- [26] H. Kahroba, B. Ramezani, H. Maadi, M.R. Sadeghi, H. Jaberie, F. Ramezani, The role of Nrf2 in neural stem/progenitors cells: From maintaining stemness and self-renewal to promoting differentiation capability and facilitating therapeutic application in neurodegenerative disease, *Ageing Res. Rev.* 65 (2021), 101211, <https://doi.org/10.1016/j.arr.2020.101211>.
- [27] X.Z. Dai, X.Q. Yan, K.A. Wintergerst, L. Cai, B.B. Keller, Y. Tan, Nrf2: redox and metabolic regulator of stem cell state and function, *Trends Mol. Med.* 26 (2) (2020) 185–200, <https://doi.org/10.1016/j.molmed.2019.09.007>.
- [28] X. Xi, Z.X. Li, H. Liu, S. Chen, D.X. Liu, Nrf2 activation is involved in cyclic mechanical stress-stimulated osteogenic differentiation in periodontal ligament stem cells via PI3K/Akt signaling and HO1-SOD2 interaction, *Front. Cell Dev. Biol.* 9 (2022), <https://doi.org/10.3389/fcell.2021.816000>.
- [29] X. Xi, Y.i. Zhao, H. Liu, Z. Li, S. Chen, D. Liu, Nrf2 activation is involved in osteogenic differentiation of periodontal ligament stem cells under cyclic mechanical stretch, *Exp. Cell Res.* 403 (2) (2021), 112598, <https://doi.org/10.1016/j.yexcr.2021.112598>.
- [30] Z.N. Yuan, J. Zhang, Y. Huang, Y.C. Zhang, W. Liu, G.S. Wang, Q. Zhang, G. Y. Wang, Y. Yang, H. Li, G.H. Chen, NRF2 overexpression in mesenchymal stem cells induces stem-cell marker expression and enhances osteoblastic differentiation, *Biochem. Biophys. Res. Commun.* 491 (1) (2017) 228–235, <https://doi.org/10.1016/j.bbrc.2017.07.083>.
- [31] V. Karkkainen, Y. Pomeschik, E. Savchenko, H. Dhungana, A. Kurronen, S. Lehtonen, N. Naumenko, P. Tavi, A.L. Levonen, M. Yamamoto, T. Malm, J. Magga, K.M. Kanninen, J. Koistinaho, Nrf2 regulates neurogenesis and protects neural progenitor cells against Abeta toxicity, *Stem Cells* 32 (7) (2014) 1904–1916, <https://doi.org/10.1002/stem.1666>.
- [32] S. Ray, M.J. Corenblum, A. Anandhan, A. Reed, F.O. Ortiz, D.D. Zhang, C. A. Barnes, L. Madhavan, A role for Nrf2 expression in defining the aging of hippocampal neural stem cells, *Cell Transplant.* 27 (4) (2018) 589–606, <https://doi.org/10.1177/0963689718774030>.
- [33] G.H. Liu, J. Qu, K. Suzuki, E. Nivet, M. Li, N. Montserrat, F. Yi, X. Xu, S. Ruiz, W. Zhang, U. Wagner, A. Kim, B. Ren, Y. Li, A. Goebel, J. Kim, R.D. Soligalla,

- I. Dubova, J. Thompson, J. Yates 3rd, C.R. Esteban, I. Sancho-Martinez, J. C. Izpisua, Belmonte, Progressive degeneration of human neural stem cells caused by pathogenic LRRK2, *Nature* 491 (7425) (2012) 603–607, <https://doi.org/10.1038/nature11557>.
- [34] J.I. Paredes, S. Villar-Rodil, Biomolecule-assisted exfoliation and dispersion of graphene and other two-dimensional materials: a review of recent progress and applications, *Nanoscale* 8 (34) (2016) 15389–15413, <https://doi.org/10.1039/c6nr02039a>.
- [35] I. Ladran, N. Tran, A. Topol, K.J. Brennand, Neural stem and progenitor cells in health and disease, *Wiley Interdiscip. Rev. Syst. Biol. Med.* 5 (6) (2013) 701–715, <https://doi.org/10.1002/wsbm.1239>.
- [36] J. Zhang, N. Kang, X. Yu, Y. Ma, X. Pang, Radial extracorporeal shock wave therapy enhances the proliferation and differentiation of neural stem cells by notch, PI3K/AKT, and Wnt/beta-catenin signaling, *Sci. Rep.* 7 (1) (2017) 15321, <https://doi.org/10.1038/s41598-017-15662-5>.
- [37] D. Frey, T. Laux, L. Xu, C. Schneider, P. Caroni, Shared and unique roles of CAP23 and GAP43 in actin regulation, neurite outgrowth, and anatomical plasticity, *J. Cell Biol.* 149 (7) (2000) 1443–1454, <https://doi.org/10.1083/jcb.149.7.1443>.
- [38] Y. Liu, P. Gao, T. Zhang, X. Zhu, M. Zhang, M. Chen, P. Du, G.W. Wang, H. Ji, J. Yang, S. Yang, Azide passivation of black phosphorus nanosheets: covalent functionalization affords ambient stability enhancement, *Angew. Chem. Int. Ed. Engl.* 58 (5) (2019) 1479–1483, <https://doi.org/10.1002/anie.201813218>.
- [39] D.M. Basso, M.S. Beattie, J.C. Bresnahan, A sensitive and reliable locomotor rating scale for open field testing in rats, *J. Neurotrauma* 12 (1) (1995) 1–21, <https://doi.org/10.1089/neu.1995.12.1>.
- [40] D.M. Basso, M.S. Beattie, J.C. Bresnahan, Graded histological and locomotor outcomes after spinal cord contusion using the NYU weight-drop device versus transection, *Exp. Neurol.* 139 (2) (1996) 244–256, <https://doi.org/10.1006/exnr.1996.0098>.
- [41] V. Chhor, R. Moretti, T. Le Charpentier, S. Sigaut, S. Lebon, L. Schwendimann, M. V. Ore, C. Zuiani, V. Milan, J. Josserand, R. Vontell, J. Pansiot, V. Degos, C. Ikonomidou, L. Titomanlio, H. Hagberg, P. Gressens, B. Fleiss, Role of microglia in a mouse model of paediatric traumatic brain injury, *Brain Behav. Immun.* 63 (2017) 197–209, <https://doi.org/10.1016/j.bbi.2016.11.001>.
- [42] K. Saijo, C.K. Glass, Microglial cell origin and phenotypes in health and disease, *Nat. Rev. Immunol.* 11 (11) (2011) 775–787, <https://doi.org/10.1038/nri3086>.
- [43] S.A. Wolf, H.W. Boddeke, H. Kettenmann, Microglia in physiology and disease, *Annu. Rev. Physiol.* 79 (2017) 619–643, <https://doi.org/10.1146/annurev-physiol-022516-034406>.